MECHANICAL

TECHNOLOGY

INCORPORATED

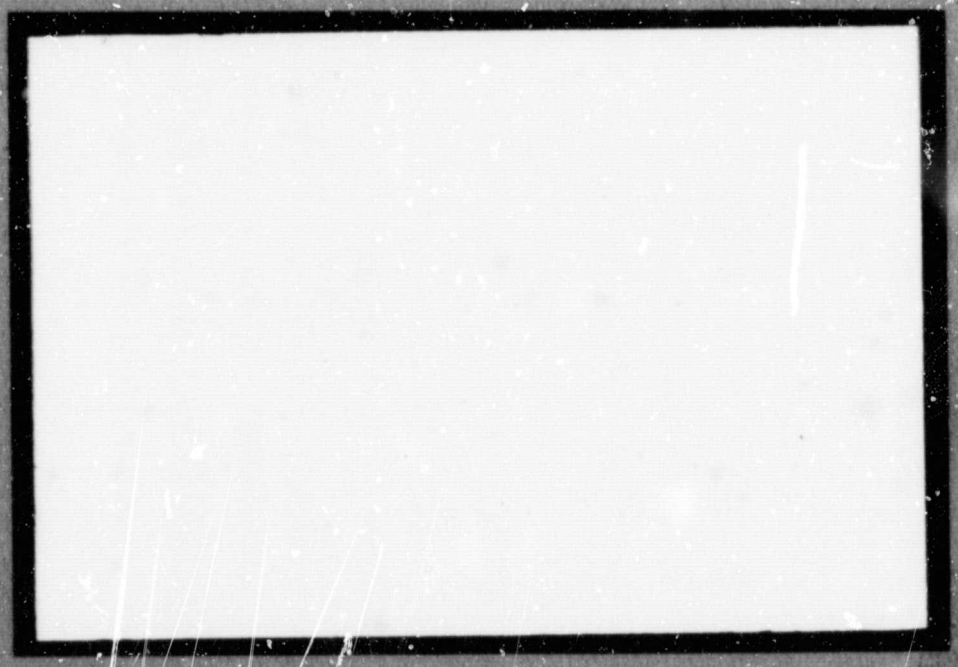

MECHANICAL TECHNOLOGY INCORPORATED
968 Albany-Shaker Road
Latham, New York 12110

MTI-67TR15

PERFORMANCE CHARACTERISTICS OF HERRINGBONE-GROOVED JOURNAL BEARINGS OPERATING AT HIGH ECCENTRICITY RATIOS AND WITH MISALIGNMENT

by

V. Castelli

J.H. Vohr

March, 1967

NO. MTI-67TR15

DATE: March, 1967

TECHNICAL REPORT

PERFORMANCE CHARACTERISTICS OF HERRINGBONE-GROOVED JOURNAL BEARINGS OPERATING AT HIGH ECCENTRICITY RATIOS AND WITH MISALIGNMENT

Vittorio Castelli John W. Cole

Author (s)

Carlos H. T. Pan

Approved

Approved

Prepared under

Contract Nonr-3730(00)

Task NR 062-317/4-7-66

Prepared for

DEPARTMENT OF DEFENSE

ATOMIC ENERGY COMMISSION

NATIONAL AERONAUTICS AND SPACE ADMINISTRATION

Administered by

OFFICE OR NAVAL RESEARCH

Department of the Navy

MTI

MECHANICAL TECHNOLOGY INCORPORATED

968 ALBANY - SHAKER ROAD — LATHAM, NEW YORK — PHONE 785-0922

TABLE OF CONTENTS

INTRODUCTION

It has been shown in recent papers by Vohr and Chow [Ref. 1], Hirs [Ref. 2] and Malanoski [Ref. 3] that spiral-grooved, journal bearings have performance characteristics which are significantly better than those possessed by plain journal bearings. A particularly important asset of gas-lubricated spiral-grooved bearings is that they are capable of high stiffness and high load capacity at high Λ operation are due to the "self pressurizing"effect of the spiral grooves.

Because the differential equation derived for the pressure distribution around a spiral-grooved bearing is such a complicated one, the only solutions to the equation obtained to date have been based on perturbation analysis, and are valid for small radial displacements only. These solutions have proved valuable in providing basic design information on spiral-grooved bearings, and because of their relative computation ease, will probably continue to be extensively used to obtain optimization design data. However, in using small displacements solutions, the question necessarily arises as to how accurately they apply to bearings operating at moderate to high eccentricity ratios. A second question that arises is whether the values of groove parameters which produce optimum performance at low eccentricities will also provide optimum performance at large displacements.

In order to resolve these and other questions, a numerical solution for the pressure distribution in a spiral-grooved bearing was obtained valid for arbitrary displacement and misalignment of the journal. Results of that solution are presented in this paper. These include performance charts, giving the load capacity and attitude angle characteristics for one optimized configuration of grooved bearing as a function of eccentricity ratio and bearing number Λ.

Other aspects of grooved bearings on which data are given are: the effect of length to diameter ratio on bearing load and attitude angle, the restoring moment generated by misalignment of the journal, the variation of optimum

values of groove parameters with eccentricity ratio and the effect of groove depth on the linearity of the load vs. eccentricity curve.

Present theoretical results are compared with recent experimental data of Malanoski.

THEORETICAL AND NUMERICAL TREATMENT

The data presented in this paper are the result of a numerical solution of an approximate form of Reynolds equation applicable to spiral groove geometries with a large number of grooves. This equation was established by J. H. Vohr and C. Y. Chow [Ref. 1] and has as the dependent variable the "smoothed" pressure distribution. The basic approximation made in the derivation is that the actual pressure distribution deviates from the smoothed one by some small amount over each ridge-groove pair and that the detailed shape of the deviation becomes unimportant as the number of grooves approaches infinity. The detailed pressure gradient components over each of the ridges and grooves are considered constant so that the flow can be calculated and related to the smoothed pressure profile.

With the nomenclature introduced by Fig. 1, the smoothed pressure equation assumes the following form:

$$\frac{1}{R}\frac{\partial}{\partial\theta}\left[(M_\theta)_r \sin\beta + (M_z)_g \alpha\cos\beta - (M_z)_r \alpha\cos\beta - \rho V h_r \sin\beta\right] + \frac{\partial}{\partial z}\left[(M_z)_g \alpha + (M_z)_r(1-\alpha)\right]\sin\beta + \left(\frac{\partial}{\partial t} + \frac{V}{R}\frac{\partial}{\partial\theta}\right)\rho\sin\beta\left[\alpha h_g + (1-\alpha)h_r\right] = 0 \qquad (1)$$

where the M's are the flow rates in the θ and z directions in the ridges and grooves; they are related to the pressure distribution by the following relations:

$$(M_\theta) = -\frac{\rho}{12\mu}\frac{h_r^3}{\alpha h_r^3 + (1-\alpha)h_g^3}\left[\left[h_g^3 - \alpha(h_g^3 - h_r^3)\cos^2\beta\right]\right.$$

$$\times \frac{1}{R}\frac{\partial\overline{P}}{\partial\theta} - \alpha(h_g^3 - h_r^3)\cos\beta\sin\beta\frac{\partial\overline{P}}{\partial z}$$

$$\left. - \alpha 6\mu(U-V)(h_g - h_r)\sin^2\beta\right] + \frac{\rho h_r}{2}(U+V) \qquad (2)$$

$$(M_z)_r = -\frac{\rho}{12\mu}\frac{h_r^3}{\alpha h_r^3 + (1-\alpha)h_g^3}\left[-\alpha(h_g^3 - h_r^3)\cos\beta\sin\beta\right.$$

$$\times \frac{1}{R}\frac{\partial\overline{P}}{\partial\theta} + \left[\alpha h_r^3 + (1-\alpha)h_g^3 + \alpha(h_g^3 - h_r^3)\cos^2\beta\right]\frac{\partial\overline{P}}{\partial z}$$

$$\left. + \alpha 6\mu(U-V)(h_g - h_r)\cos\beta\sin\beta\right] \qquad (3)$$

$$(M_\theta)_g = -\frac{\rho}{12\mu}\frac{h_g^3}{\alpha h_r^3 + (1-\alpha)h_g^3}\left[\left[h_r^3 + (1-\alpha)(h_g^3 - h_r^3)\right.\right.$$

$$\left.\times \cos^2\beta\right]\frac{1}{R}\frac{\partial\overline{P}}{\partial\theta} + (1-\alpha)(h_g^3 - h_r^3)\cos\beta\sin\beta\frac{\partial\overline{P}}{\partial z}$$

$$\left. + (1-\alpha)6\mu(U-V)(h_g - h_r)\sin^2\beta\right] + \frac{\rho h_g}{2}(U+V) \qquad (4)$$

$$(M_z)_g = -\frac{\rho}{12\mu}\frac{h_g^3}{\alpha h_r^3 + (1-\alpha)h_g^3}\left[(1-\alpha)(h_g^3 - h_r^3)\cos\beta\right.$$

$$\times \sin\beta\frac{1}{R}\frac{\partial\overline{P}}{\partial\theta} + \left[\alpha h_r^3 + (1-\alpha)h_g^3 - (1-\alpha)(h_g^3 - h_r^3)\right.$$

$$\left.\left.\times \cos^2\beta\right]\frac{\partial\overline{P}}{\partial z} - (1-\alpha)6\mu(U-V)(h_g - h_r)\cos\beta\sin\beta\right] \qquad (5)$$

In the present treatment, the speeds U and V and the clearances h_r and h_g were specialized to the following forms:

$$V = R\omega_1 \tag{6}$$

$$U = R\omega_2 \tag{7}$$

$$h_r = C + (x_o + \alpha_1 z) \sin\theta + (y_o + \alpha_2 z) \cos\theta \tag{8}$$

$$h_g = h_r + \Delta \tag{9}$$

where Δ = groove depth = constant.

The values of x_o and y_o represent the coordinates of the shaft center at z = 0 measured with respect to the concentric position. The angles α_1, and α_2 allow misalignment of the shaft and bearing axes. The geometry is presented in Fig. 2.

The numerical treatment of Eq. (1) follows the method introduced in references 5 and 6.

Eq. (1) is a second order partial differential equation with variable coefficients and contains the first derivative of density with respect to time. The difference between this equation and all other forms of Reynolds equation encountered in the literature is in the presence of the cross, second space derivative $\frac{\partial^2 P}{\partial z \partial \theta}$.

The assumption that the film is isothermal leads to the replacement of the density by the pressure P throughout. The equation is now non-linear, containing P^2 as well as P.

The change in variables

$$Q = P^2 \tag{10}$$

leads to the same form of equation in Q with the quantity $\sqrt{Q}$ in some of the

coefficients.

Approximating all space derivatives of Q by standard central difference formulae and the time derivative by a forward difference formula, equation (1) becomes algebraic, involving, at each point of a finite cell mesh drawn on the gas film, the value of Q at the point and its eight immediate neighbors.

Letting the value of $\sqrt{Q}$ at each grid point be a part of the coefficients, (imagining that it is known) the resulting algebraic equations are linear in Q.

Due to the fact that none of the central differences introduce points further away from the center point than one column and one row, equation (1) reduces to the form

$$[A]_j \{Q\}_j + [B]_j \{Q\}_{j-1} + [C]_j \{Q\}_{j+1} = \{R\}_j \; ; \quad j = 1,N \tag{11}$$

where, for each value of j, the M equations pertaining to an entire column of points (i = 1, 2, ...M) are written at once. Therefore, each matrix equation (11) contains M equations thus making the dimensions of $[A]_j$, $[B]_j$, $[C]_j$ be M x M and the dimensions of $\{R\}_j$ be M.

It should be noted that equation (11) can also be used for boundary points as long as the proper values are inserted in the coefficient matrices and the right hand side. This is shown below.

The boundary conditions are of the following types:

a) given pressure (such as ambient) at the bearing ends.

$$Q_{i,j} = P_a^2 \tag{12}$$

Equation (12) is of the same general type as equation (11) so that this type of boundary condition can be formulated together with the field equations.

b) flow matching between two grooved regions of different characteristics. This includes the case of grooved regions adjacent to plain regions due to the fact that, if $\Delta = 0$, equation (1) reduces to the equation valid for plain bearings.

The present treatment is limited to cases where dissimilar grooved regions are joined on lines of constant z. Then the conditions can be expressed as

$$\left[(M_z)_g \, \alpha + (M_z)_r \, (1 - \alpha) \right]_-^+ = 0 \tag{13}$$

where + and - mean the two sides of the joint line. The derivatives of pressure implied by (13) on either side of the joint line are written by means of two point formulae so that also equation (13) involves the joint point and its immediate neighbors and can be written in the same form as equation (11).

c) lines of symmetry. These only occur at z = constant (center plane of bearing). This condition means that no flow in the z direction can exist at any θ position or

$$(M_z)_g \, \alpha + (M_z)_r \, (1 - \alpha) = 0 \tag{14}$$

which can be used by writing the regular field equation at the symmetry point and eliminating all values of Q at the points on the non-treated side of the boundary by means of equation (14).

d) cyclic condition

$$P(\theta) = P(\theta + 2\pi) \tag{15}$$

$$\frac{\partial P}{\partial \theta} \, (\theta) = \frac{\partial P}{\partial \theta} \, (\theta + 2\pi) \tag{16}$$

Letting j vary in the θ direction, equations (15) and (16) reduce to the following:

$$\{Q\}_1 = \{Q\}_{N+1} \tag{17}$$

$$\{Q\}_0 = \{Q\}_N \tag{18}$$

However, equations (17) and (18) introduce two difficulties: first, they do not relate three or less adjacent columns of unknowns, and second, they introduce $\{Q\}_{N+1}$ and $\{Q\}_0$ which are outside of the grid of unknowns. Reference [2] suggests how to write the regular field equations on columns 1 and N and gives a procedure for satisfying the boundary conditions (17) and (18).

Therefore, the columnwise influence coefficient methods introduced in Reference [2] can now be used to solve equation (11).

Two solution strategies can be followed:

a) Iteration method. The time derivative is set to zero, the value of $\sqrt{Q}$ in the coefficients is started at some guess, the value of Q is found at each grid point by solving equation (11), this value is used in $\sqrt{Q}$ and the answer is obtained by iteration. This method is quite efficient when it converges because it usually gains one digit accuracy every one or two iterations. However, for severe conditions of eccentricity and bearing parameter Λ, severe numerical instability hinders the success of this method of solution.

b) Diffusion method: the time derivative is left in equation (1), an initial distribution of Q is selected and used to evaluate the $\sqrt{Q}$ terms, and equation (11) is then solved repeatedly to find Q (ΔT), Q (2ΔT).... where ΔT represents a suitable time step. Therefore, the progress of the pressure distribution in time is followed as in the natural diffusion process by which the pressure adjusts to a change in running conditions. The asymptotic value of the pressure at any point is that corresponding to steady-state. This method can always be made numerically stable by choice of a suitably small value of ΔT. Therefore, although more computing time

is necessary, answers can be gotten even for severe running conditions.

The output data include the integrals of the pressure distribution so that the resultant forces along the x and y axes and the resultant moments about the same axes are known.

$$F_x = \int\int P \sin\theta \, r dz d\theta \tag{19}$$

$$F_y = \int\int P \cos\theta \, r dz d\theta \tag{20}$$

$$M_x = -\int\int Pz \cos\theta \, r dz d\theta \tag{21}$$

$$M_y = \int\int Pz \sin\theta \, r dz d\theta \tag{22}$$

The computer program used for implementation of the solution scheme is written in FORTRAN IV, and can accomodate slider bearings as well as journal bearings.

RESULTS

Steady-state, radial displacement, performance data calculated for the spiral-grooved journal bearing are shown in Figs. 3 and 4. Fig. 3 presents the dimensionless load $\overline{W} = \frac{W}{P_a LD}$ vs. bearing number $\Lambda = \frac{6\mu\omega}{P_a}(\frac{R}{C})^2$ for various values of eccentricity ratio ϵ while Fig. 4 presents data on the bearing attitude angle ϕ as a function of Λ and ϵ. The data presented are for a bearing of L/D = 1.0, with grooved member rotating, having the following values for the groove parameters.

$\beta = 25°$
$\alpha = 0.35$ (optimum groove parameters for maximum radial load at $\Lambda = 20$)
$\Gamma = 2.33$
$\overline{Z} = 0.5$

These are the optimum values to provide maximum radial stiffness* at $\Lambda = 20$ and $\epsilon = 0$ for the case of grooved member rotating. This particular bearing was chosen for high eccentricity analysis because it had been studied experimentally [Ref. 3] and a stability chart had been prepared for it. It should be noted that optimum groove geometry for maximum stiffness at other values of Λ are not too different from those presented above. Optimum values for groove parameters are somewhat different if the smooth member rotates rather than the grooved member. In this paper, all data reported are for the case of grooved member rotating.

In Fig. 5 is compared the load vs. eccentricity and attitude angle characteristics of a plain bearing and our spiral-grooved bearing at $\Lambda = 9.0$. The plain bearing data were obtained from a study by Raimondi [Ref. 7] As can be seen, the non-linear increase of load with eccentricity for the optimized grooved bearing is very nearly the same as for the plain bearing. Also, the

---

* Radial stiffness at $\epsilon = 0$ is defined as $\frac{W \cos \phi}{\epsilon}$ where $\epsilon << 1$.

attitude angles for both bearings decrease in the same manner with ϵ. One can note, however, that the attitude angle for the grooved bearing is lower than that for the plain bearing.

When run at other values of Λ (i.e., $\Lambda = 0.1$ and $\Lambda = 1.5$) the load capacity of the grooved bearing was found to increase more rapidly with eccentricity ratio than does that of a plain bearing. As we shall see later, the linearity of the load vs. eccentricity ratio curve for spiral grooved bearings does depend on the values of the groove parameters. Hence, it is difficult to generalize about the linearity of the load curve other than to say that like plain bearings, the radial stiffness of grooved bearings does always appear to increase with eccentricity ratio.

In Fig. 6 is shown the effect of length to diameter ratio on the performance of a grooved bearing at $\Lambda = 1.5$. Increasing L/D from 1.0 to 2.0 for the grooved bearing, results in an increase in dimensionless load of 90%. In comparison, the increase for a plain bearing would be only 75%. The greater percentage increase obtained for the grooved bearing is probably due to its self-pressurizing effect, which would be greater as length increases. One would expect this effect to be more significant at higher values of Λ and to be insignificant as $\Lambda \rightarrow 0$.

In the present study, the moment M that would develop on the journal due to misalignment was calculated for one value of $\Lambda(\Lambda = 1.5)$. The results are shown in Fig. 7. The abscissa in this figure is $\delta L/C$ where δ is the angle of misalignment in radians. $\delta L/C$ represents the change in eccentricity ratio from one end of the bearing to the other. Also shown in Fig. 7 are misalignment moments for a plain bearing obtained from a linear perturbation analysis by Ausman [Ref. 8].

There are two interesting features about the data in Fig. 7. One is that the misalignment moments for the grooved bearing are very linear with δ (the moments plotted for the plain bearing are necessarily linear because they were calculated from perturbation analysis). The second is that the attitude angle of the misalignment moment is very much less for the grooved bearing than for the plain bearing (39° for the grooved bearing vs. 80° for the plain bearing). Also, the grooved bearing seems to have a larger misalignment moment relative to its load capacity than does the plain bearing. For example, the ratio of the moment, M/L at $\delta L/C = 0.1$ to the load W at $\epsilon = 0.1$ is .0263 for the grooved bearing but only

.022 for the plain bearing. These ratios can be used to estimate misalignment moments from load data for bearings with L/D = 1.0 if misalignment data is unavailable.

An important question concerning the performance of grooved bearings at high eccentricity is whether the values of groove parameters that yield maximum radial load at low eccentricities will also give maximum radial load at high eccentricity. To investigate this, we determined the groove parameters to give maximum radial load for $\epsilon << 1$ at $\Lambda = 0.1$, and then studied the effect that changes in these parameters would make on radial load at $\epsilon = 0.6$. The results are presented in Fig. 8a through 8d. The optimum values for β, α, Γ and $\overline{Z}$ for $\epsilon \longrightarrow 0$ are indicated, respectively, by the dashed vertical lines in Figs. 8a through 8d. These values are:

$\beta = 29°$
$\alpha = 0.51$ (optimum groove parameters for maximum radial load at $\Lambda = 0.1$)
$\Gamma = 2.2$
$\overline{Z} = 0.765$

As can be seen in Fig. 8, the above optimum values of β, α and $\overline{Z}$ also are very close to the optimum values for $\epsilon = 0.6$. An exception is the parameter $\Gamma = (h_g/h_r)_{\epsilon = 0}$, the optimum value for which is approximately 1.8 for $\epsilon = 0.6$. That the optimum value of Γ should decrease with eccentricity is quite reasonable physically. It follows from the fact that to maximize bearing load at high ϵ, one would want h_g/h_r to be at optimum value in the narrow clearance region where the load carrying pressure profile is developed. To keep h_g/h_r at a local optimum value in a region where h_g and h_r are becoming smaller, one would have to reduce $h_g - h_r$ i.e. reduce $\Gamma = (h_g/h_r)_{\epsilon = 0}$.

If one used a value of 1.8 for Γ in the design of a grooved bearing at $\Lambda = 0.1$, the radial load at low eccentricity would be reduced below that obtained with $\Gamma = 2.2$ whereas the load at $\epsilon = 0.6$ would be increased. Hence, the load vs. eccentricity curve would be even less linear than it would be with $\Gamma = 2.2$. The reverse possibility also exists. That is, by using a value of Γ greater than 2.2 one should reduce load capacity more at high ϵ than at low ϵ and

produce a more linear load vs. ϵ curve. This performance characteristic would be desirable in many bearing applications e.g. gyroscope suspension systems.

To try to improve the linearity of the load vs. ϵ curve, calculations were made using $\Gamma = 2.8$ and 3.2. As an index of linearity we can form the ratio $\frac{(W)_{\epsilon = 0.6}}{(W)_{\epsilon = 0.3}}$. With perfect linearity, this ratio would be 2. From our calculations we obtain that this ratio is 2.3 for $\Gamma = 2.8$ and 2.18 for $\Gamma = 3.2$. For $\Gamma = 2.2$, the ratio is 2.57. We thus find that increasing Γ does significantly improve the linearity of the load vs. ϵ curve.

The above example points up one of the important advantages of spiral-grooved bearings, namely, their flexibility to be designed to satisfy many different performance requirements by proper choice of the groove parameters. Of course, this is not without its drawbacks. Due to the many design variables associated with spiral-grooved bearings, proper design of these bearings can be a very complicated task.

Before leaving the discussion of optimum values for β, α, Γ and $\bar{Z}$, we can note that the optimum values of these parameters for $\Lambda = 0.1$ are not too different from the optimum values for $\Lambda = 20$. More significantly, the bearing optimized for radial load at $\Lambda = 20$, when run at $\Lambda = 0.1$, has only 13% less radial load capacity than the bearing optimized specifically for operation at $\Lambda = 0.1$. Hence this $\Lambda = 20$ design can give satisfactory performance over a wide range of Λ.

As noted earlier, experimental data have been obtained by Malanoski [Ref. 3] for the spiral-grooved bearing optimized for maximum stiffness at $\Lambda = 20$. The load vs. eccentricity data are shown in Fig. 9 along with the appropriate theoretical curves obtained from Fig. 3. Two test bearings were used, each of length and diameter equal to 1.5 inches with 36 spiral grooves etched onto the journal surface.

As can be seen, agreement between experiment and the[ory] is quite good at all

values of Λ up to 15.5, with the unexplained exception of the data taken at $\Lambda = 2.68$, which is quite a bit lower than theory predicts. The fact that all data lie somewhat below the theoretical curves can be partly explained by the so called "edge effect" considered by Muidjerman [Ref. 9] for incompressible thrust bearings. The predicted degradation of load due to edge effect in Malanoski's bearing, as calculated from [Ref. 10], would be 8%.

In Table 1 below the values of attitude angle measured by Malanoski at higher values of eccentricity are compared with theoretical values obtained from the curves. in Fig. 4.

TABLE 1

Comparison of Predicted and Measured
Attitude Angles for Spiral Grooved Bearing
L/D = 1.0, $\beta = 25°$, $\alpha = 0.35$, $\Gamma = 2.33$, $\bar{Z} = 0.5$

Λ	ϵ	Attitude Angle Expt	Attitude Angle Theory
1.25	.396	58°	52°
1.25	.523	58°	47°
2.68	.327	50.5°	41.5°
2.68	.487	48.5°	36°
8.47	.269	21.6°	17°
8.47	.310	23.5°	16.5°
15.5	.27	11.2°	7°
15.5	.333	9.1°	6.5°

In general, agreement between theory and measurement is reasonably good although measured values of attitude angle are consistently larger than predicted.

For sake of completeness, we have included in this paper a stability map for the spiral-grooved bearing tested by Malanoski. This map is

shown in Fig. 10. Discussion of the theoretical basis for this map is beyond the scope of this present paper; the interested reader is referred to the papers by Pan [Ref. 4] and by Malanoski [Ref. 3] for details of the analysis leading to construction of the map.

The ordinates for Fig. 10 are bearing number Λ and bearing dimensionless critical mass $\overline{M}_c$. Use of the map for design purposes is very simple: one simply determines the bearing number Λ at which one plans to operate, and then calculates the maximum value of critical mass corresponding to that Λ. Actual rotor mass must be less than this value for stability.

Alternatively, one may enter Fig. 10 with a dimensionless critical mass, and determine the maximum value of Λ at which the bearing can operate stably.

The stability data in Fig. 10 pertains to unloaded bearings operating at $\epsilon = 0$. Limited experimental data indicates that loading the bearing improves its stability. [Ref. 11].

Full experimental verification of the stability map in Fig. 10 has not been achieved. However, the test bearing of Malanoski was run unloaded at 60,000 RPM($\Lambda = 20$) with no sign of instability. The rotor mass was 2.125 lbs. per bearing which gave a value for the dimensionless mass parameter of 0.2. Predicted critical speed for the bearing was approximately 80,000 RPM.

SUMMARY AND CONCLUSIONS

A solution for the pressure distribution around a spiral-grooved journal bearing operating at large eccentricity ratios is obtained numerically by the method of influence coefficients. Performance charts giving load capacity and attitude angle are provided for a bearing optimized for radial stiffness at $\Lambda = 20$ for the case of grooved member rotating. The charts cover the range of Λ from 0.1 to 20. Curves are given for eccentricity ratios up to $\epsilon = 0.7$. The bearing considered has good load carrying capabilities over the entire range covered by the performance charts and is therefore a useful design. A stability map is provided for the bearing.

It is found that the load capacity of a spiral-grooved journal bearing optimized for maximum radial stiffness increases non-linearly with eccentricity ratio in qualitatively the same fashion as does the load capacity of a plain bearing. Also, the attitude angle for grooved bearings decreases with eccentricity in essentially the same manner as for plain bearings. Hence, it is tentatively recommended that in cases where only low eccentricity data is available on a grooved bearing, this data can be extrapolated to high eccentricity by assuming that the grooved bearing behaves similarly to a plain bearing. Calculations indicate that this would result in a conservative estimate of load capacity for the grooved bearing.

The variation of grooved bearing performance with length to diameter ratio is briefly examined. It appears that the increase in dimensionless load with L/D is greater for grooved bearings than for plain bearings.

The restoring moment generated due to misalignment of a grooved journal is found to increase approximately linearly with the angle of misalignment. The attitude angle of the restoring moment is much lower for grooved bearings than the plain bearing.

Optimum values of the grooved parameters β, α, $\overline{Z}$, to produce maximum radial stiffness at high eccentricity were found to be approximately the same as those obtained from small eccentricity analysis. However, it was found that

the optimum groove depth ratio, Γ, for maximum load at high eccentricity should be smaller than that producing maximum load at low eccentricity. It was also found that the choice of Γ significantly affected the linearity of the load vs. eccentricity,with larger values of Γ tending to make the curve more linear although with some sacrifice in load capacity. In some applications, however, linearity of bearing response may be more important than large load capacity.

ACKNOWLEDGEMENT

The authors gratefully acknowledge the assistance given by S.B. Malanoski in obtaining the data presented in this paper.

The work reported here was supported by the Office of Naval Research under Contract Nonr-3730(00), Task NR 062-317/4-7-66.

REFERENCES

1. Vohr, J.H. and Chow, C.Y., "Characteristics of Herringbone-Grooved, Gas-Lubricated Journal Bearings", Trans. ASME 64-LUB-15 Journal of Basic Engineering, Vol. 87, Ser. D. No. 3, Sept. 1965.

2. Hirs, G.G., "The Load Capacity and Stability Characteristics of Hydrodynamic Grooved Journal Bearings", ASLE Paper No. 64LC-24 presented at the ASME-ASLE International Conference in Washington, D.C., Oct., 1964.

3. Malanoski, S.B., "Experiments on an Ultrastable Gas Journal Bearing", ASME Paper No. 66-LUB-6 presented at the ASME-ASLE Lubrication Conference, Minnsapolis, Minn., Oct. 18-20, 1966.

4. Pan, C.H.T., "Spectral Analysis of Gas Bearing Systems for Stability Studies", M.T.I. Report No. 64TR58, prepared for ONR under contract Nonr-3730(00), Task No. 061-131.

5. Castelli, V. and Shapiro, W., "Improved Method for Numerical Solution of the General Incompressible Fluid Film Lubrication Problem", ASME Paper No. 66-LUBS-14, presented at ASME Lubrication Symposium, June 5-9, 1966, New Orleans, La.

6. Castelli, V. and Pirvics, J., "Equilibrium Characteristics of Axial Groove Gas Lubricated Bearings", Paper No. ASME 65-LUB-16, presented at the ASLE-ASME Lubrication Conf., Oct. 18-20, 1965, San Francisco, Cal.

7. Raimondi, A.A., "A Numerical Solution for the Gas-Lubricated Full Journal Bearing of Finite Length", Trans. ASLE, Vol. 4, 1961, pp. 131-155.

8. Ausman, J.S., "Theory and Design of Self-Acting Gas-Lubricated Journal Bearings Including Misalignment Effects", First International Symposium on Gas Lubricated Bearings, Sponsored by ONR, Dept. of the Navy, ACR-49 Edited by D.D. Fuller, Oct. 26-28, 1959, Wash. D.C., Pgs. 161-192.

9. Muijderman, E.A., "Spiral-Groove Bearings", Philips Research Reports Supplements, Philips Research Laboratories, Printed in the Netherlands, No. 2, 1964.

10. Pan, C.H.T., "Fixed Self-Acting Journal Bearings", Lecture given in RPI-MTI Gas Bearing Course held at Rensselaer Polytechnic Institute, Troy, N.Y., June 13-24, 1966.

11. Murray, F. and Wilson, D., "Gas Lubrication Research for 1900°F Non-Isothermal Operation", MTI Letter report No. 12, April, 1967, Air Force Contract AF 33(615)-3235.

NOMENCLATURE

C = Bearing clearance - in.

D = Bearing diameter - in.

F_x, F_y = Radial and tangential bearing forces - lb.

h_g = Local film thickness in groove region - in.

h_r = Local film thickness in ridge region - in.

L = Bearing length - in.

L_1 = Total length of grooved region

M = Total moment $= \sqrt{M_x^2 + M_y^2}$ - in.lb.

M_c = Critical bearing mass - $lb.sec^2/in.$

$\overline{M}_c$ = Dimensionless critical mass $= \dfrac{M_c \left(\frac{C}{R}\right)^5}{LD} \dfrac{RP_a}{\mu^2}$

M_x, M_y = Radial and tangential moments - in.lb.

$(M_\theta)_g$, $(M_z)_g$,

$(M_\theta)_r$, $(M_z)_r$ = Local groove and ridge mass flow components - lb/sec.in.

P = Pressure - lb/in^2

$\overline{P}(\theta,z)$ = Idealized, "overall" pressure distribution - lb/in^2

P_a = Ambient pressure - lb/in^2

Q = P^2 - lb^2/in^4

r,θ,z = Cylindrical coordinates

t = Time - seconds

U = Velocity of smooth member - in/sec.

V = Velocity of grooved member - in/sec.

W = Bearing total force - lb.

$\overline{W}$ = Dimensionless load $= \dfrac{W}{P_a LD}$

x_o, y_o = Coordinates of shaft center at $Z = 0$.

$\overline{Z}$ = Fraction of bearing length occupied by grooves $= L_1/L$

α = Fraction of width of groove-ridge pair that is occupied by groove

α_1, α_2 = Misalignment angles - radians

β = Groove angle - radians

Γ = Ratio of groove clearance to ridge clearance when bearing is concentric = $(h_g/h_r)_{\epsilon = 0}$

Δ = Grooved depth = $(h_g - h_r)$- in.

ΔT = Time step - seconds

δ = Total misalignment angle = $\sqrt{\alpha_1^2 + \alpha_2^2}$ - radians

ϵ = Eccentricity ratio = e/C

Λ = Compressibility number, $\frac{6\mu\omega R^2}{P_a C^2}$

μ = Viscosity - $lb.sec/in^2$

ρ = Density - lb/in^3

ϕ = Bearing attitude angle - radians

ω = Sum of rotational speeds = $\omega_1 + \omega_2$ - radians/sec.

ω_1 = Rotational speed of grooved member - radians/sec.

ω_2 = Rotational speed of smooth member - radians/sec.

LIST OF FIGURES

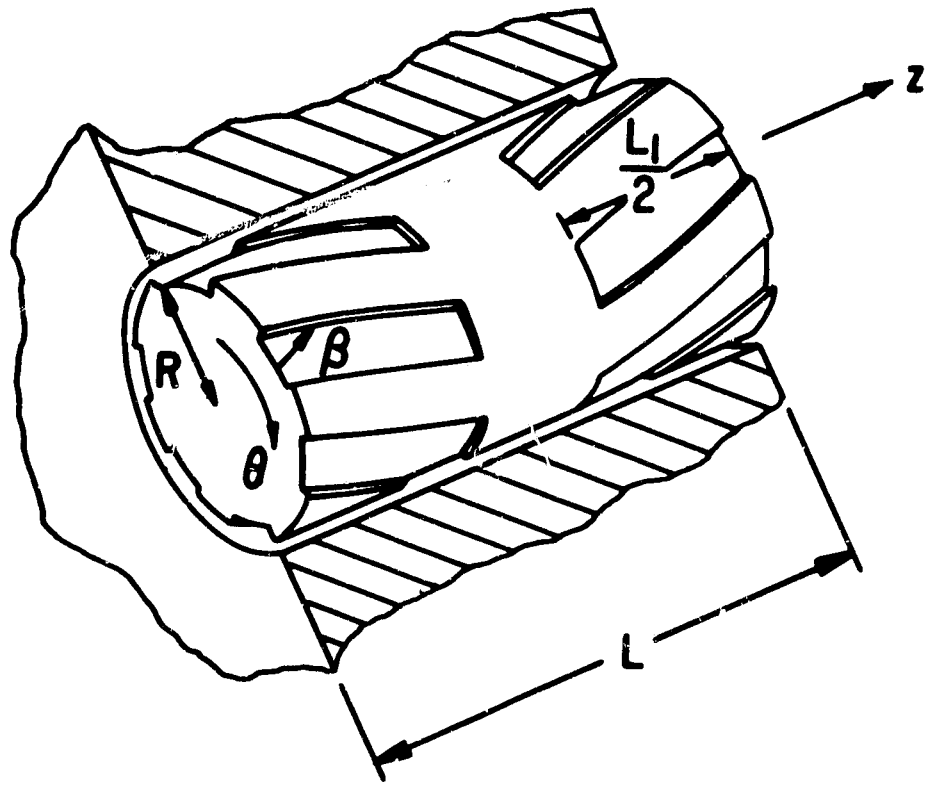

$$\alpha = \frac{a_g}{a_g + a_r}$$

$$\Gamma = \frac{h_g}{h_r}$$

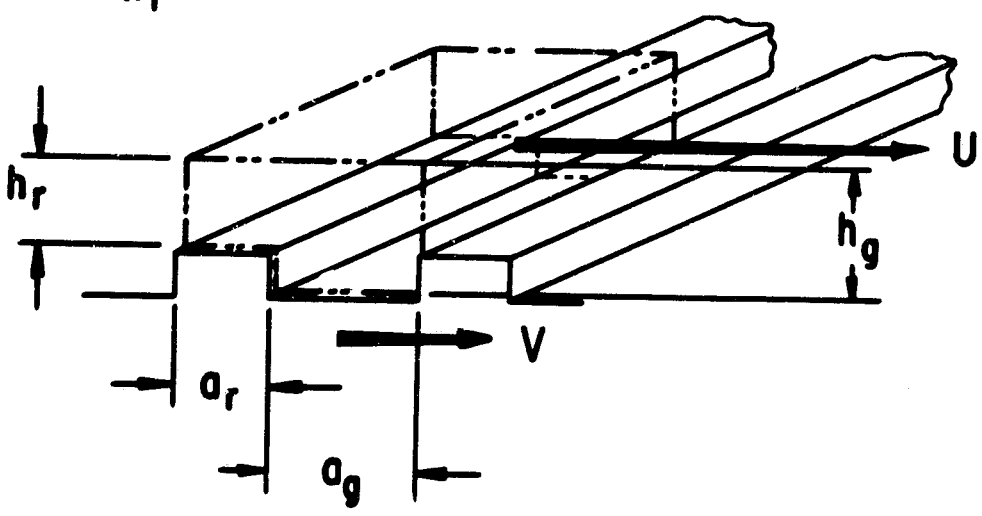

Fig. 1 Geometry of Spiral-Grooved Journal Bearing

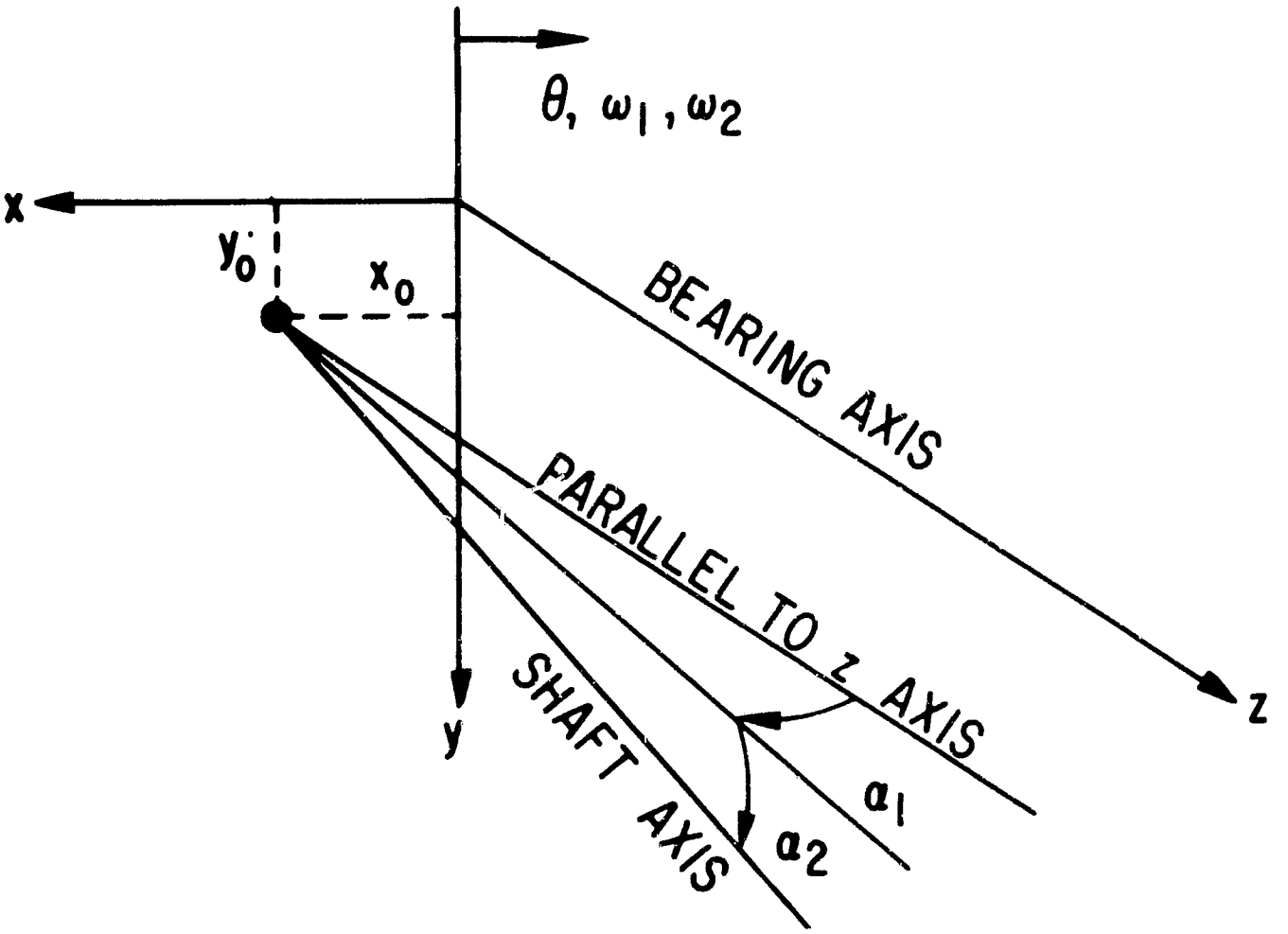

Fig. 2 Locating Coordinates for Bearing

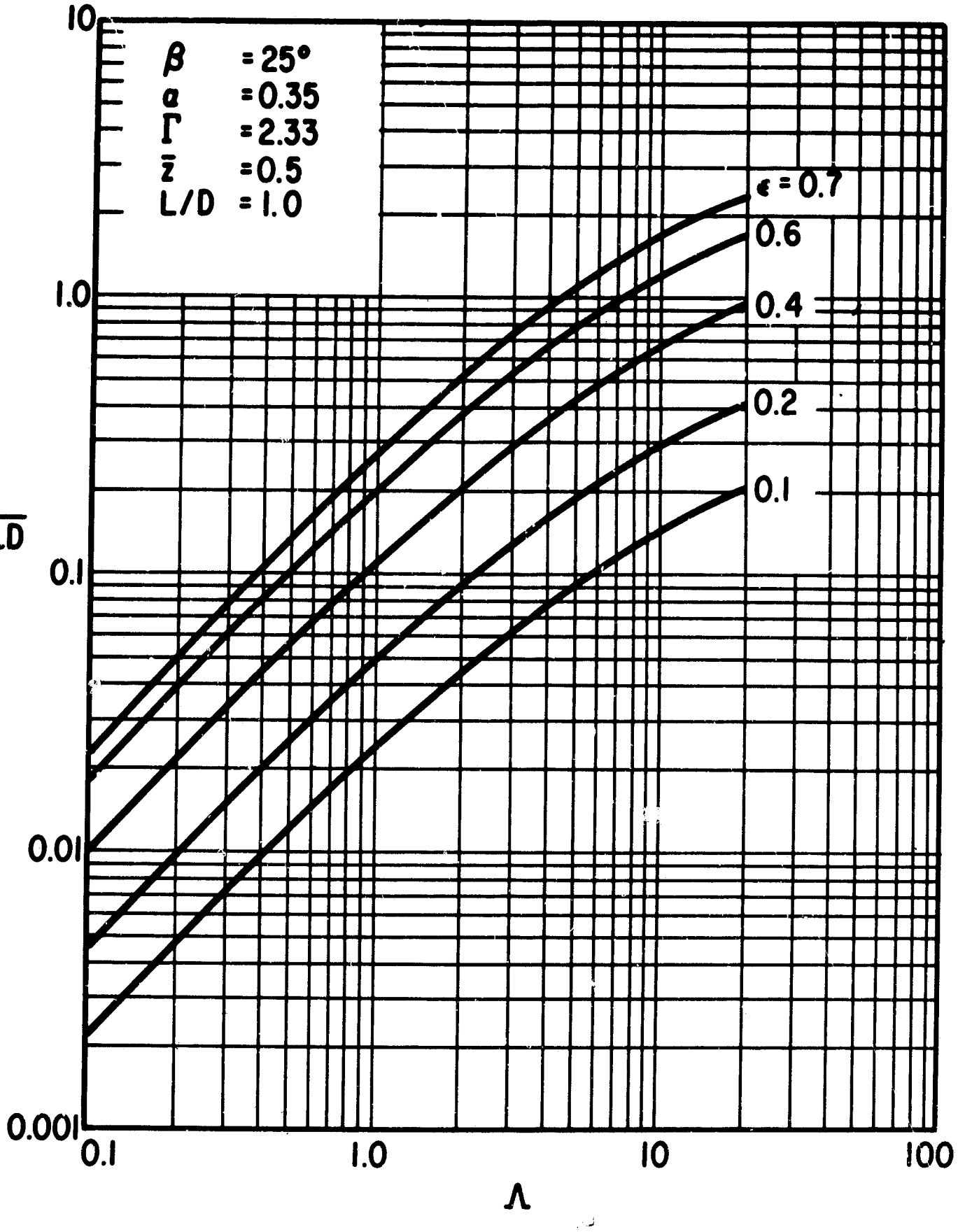

Fig. 3 Load Capacity of Spiral-Grooved Journal Bearing as a Function of Bearing Number $\Lambda = \frac{6\mu\omega}{P_a}\left(\frac{R}{C}\right)^2$ and Eccentricity Ratio

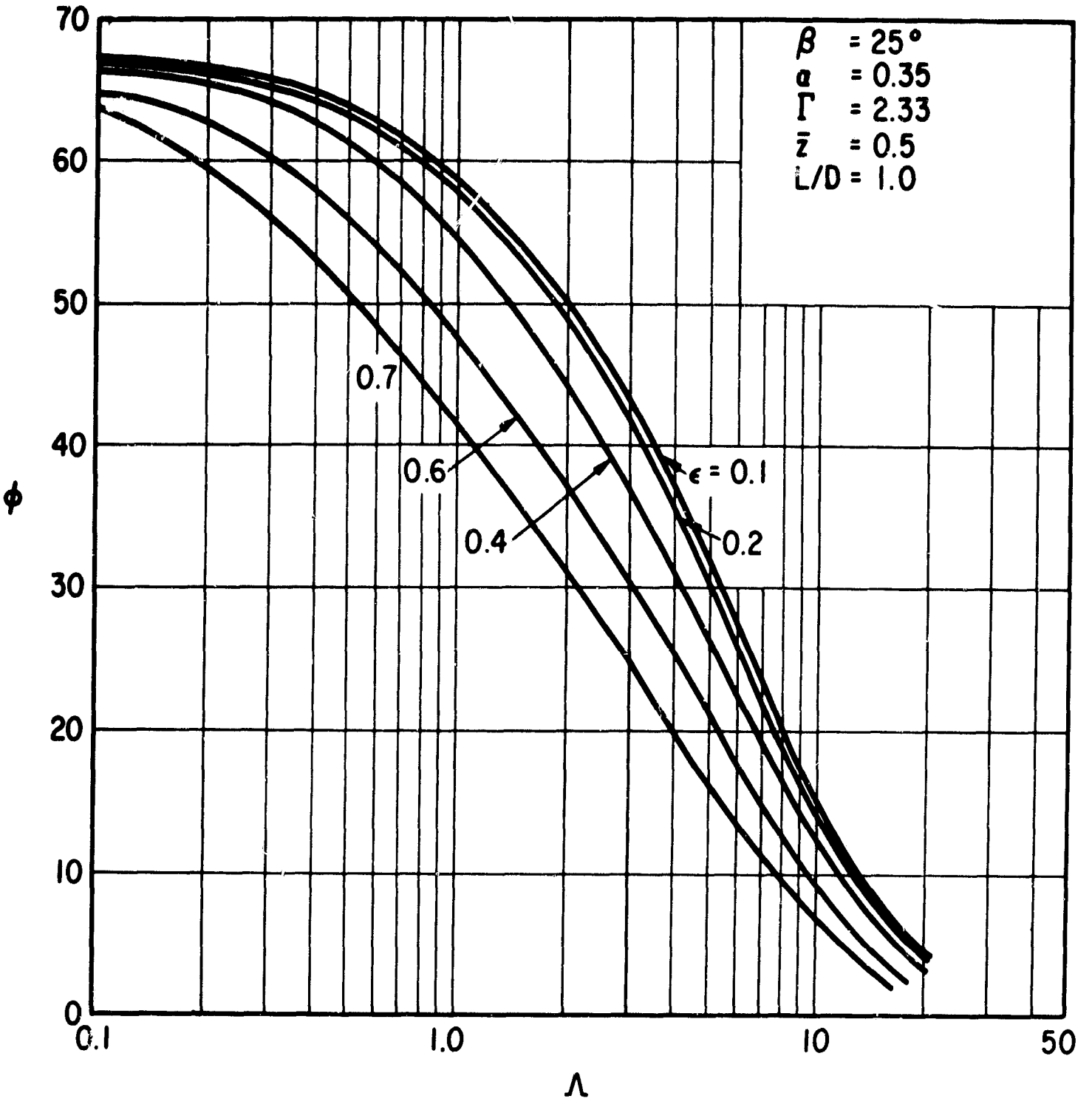

Fig. 4 Attitude Angle of Spiral-Grooved Journal Bearing as a Function of Bearing Number $\Lambda = \frac{6\mu\omega}{P_a}\left(\frac{R}{C}\right)^2$ and Eccentricity Ratio

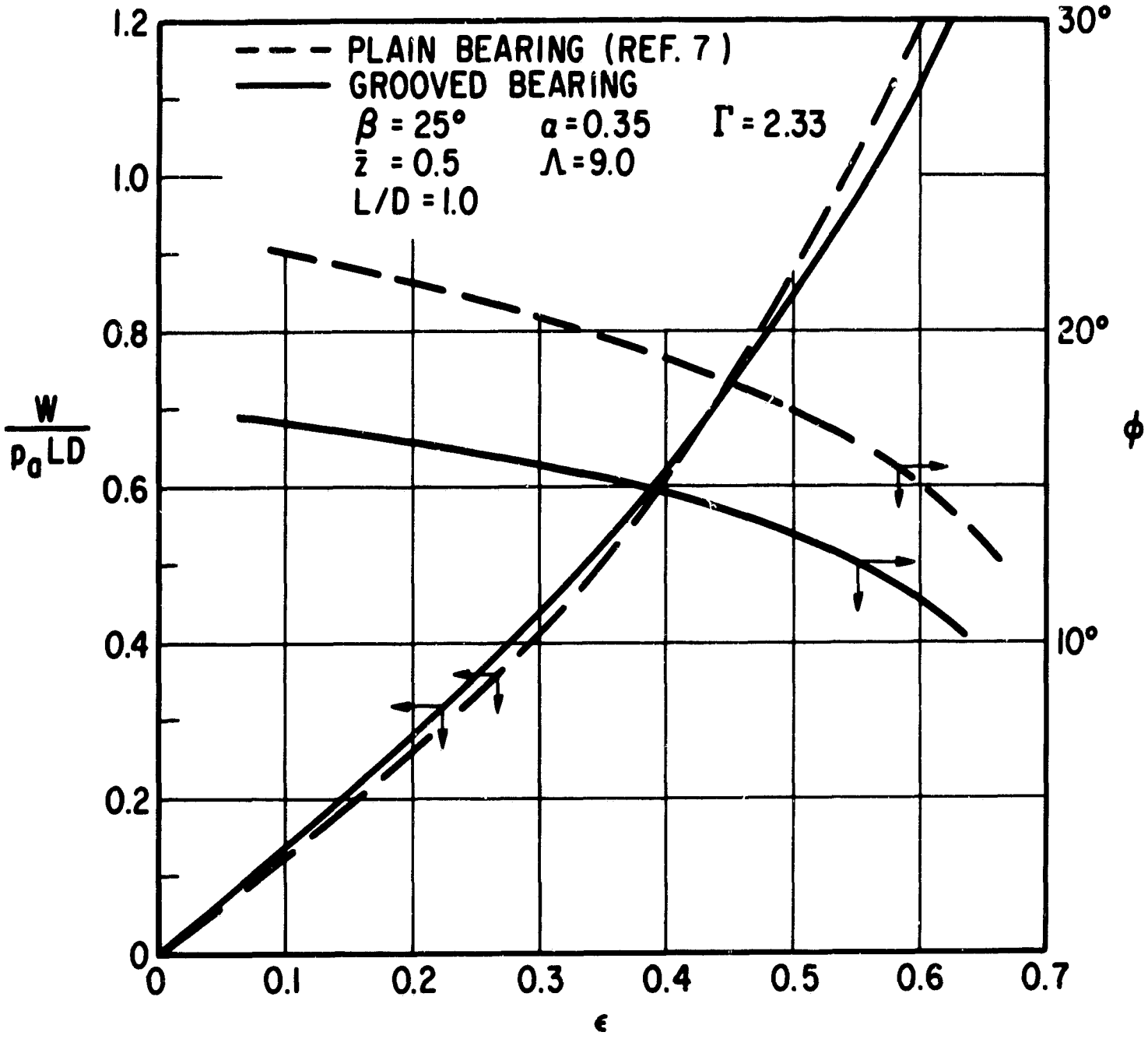

Fig. 5 Comparison of Load Capacity and Attitude Angle Characteristics for Spiral-Grooved and Plain Bearing

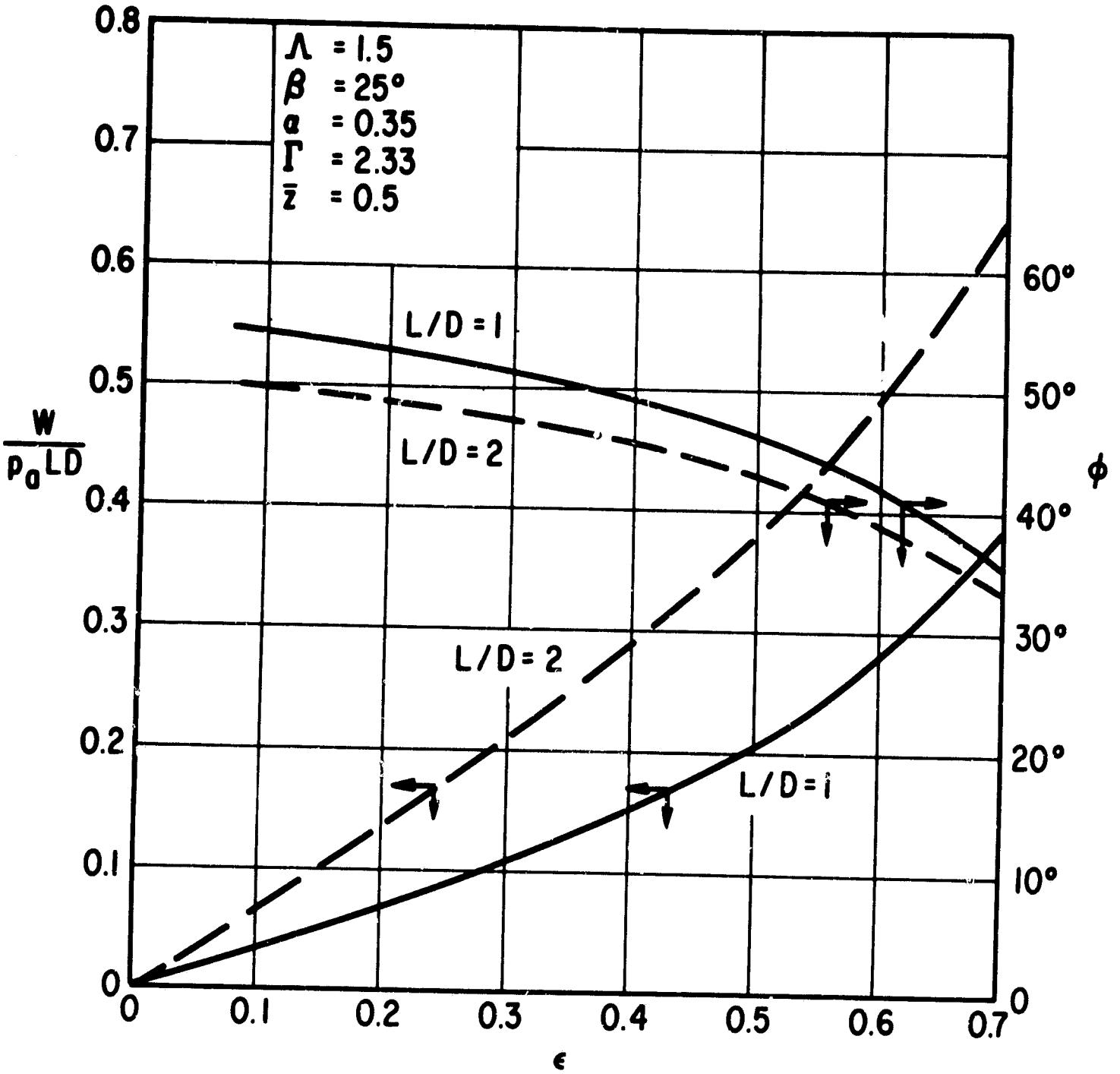

Fig. 6 Effect of L/D Ratio on Performance of Spiral-Grooved Bearing

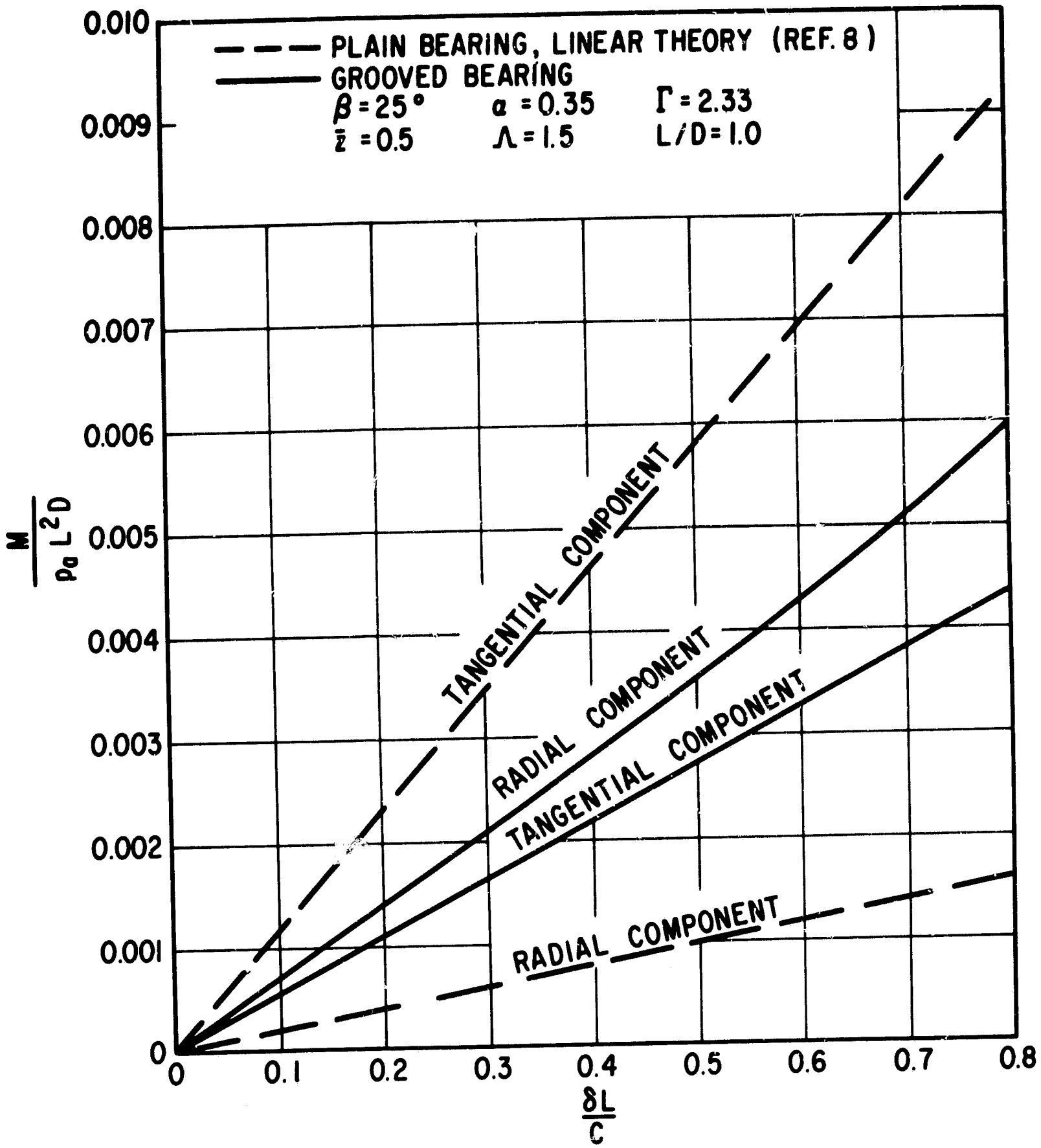

Fig. 7 Misalignment Movements for Spiral-Grooved and Plain Bearings

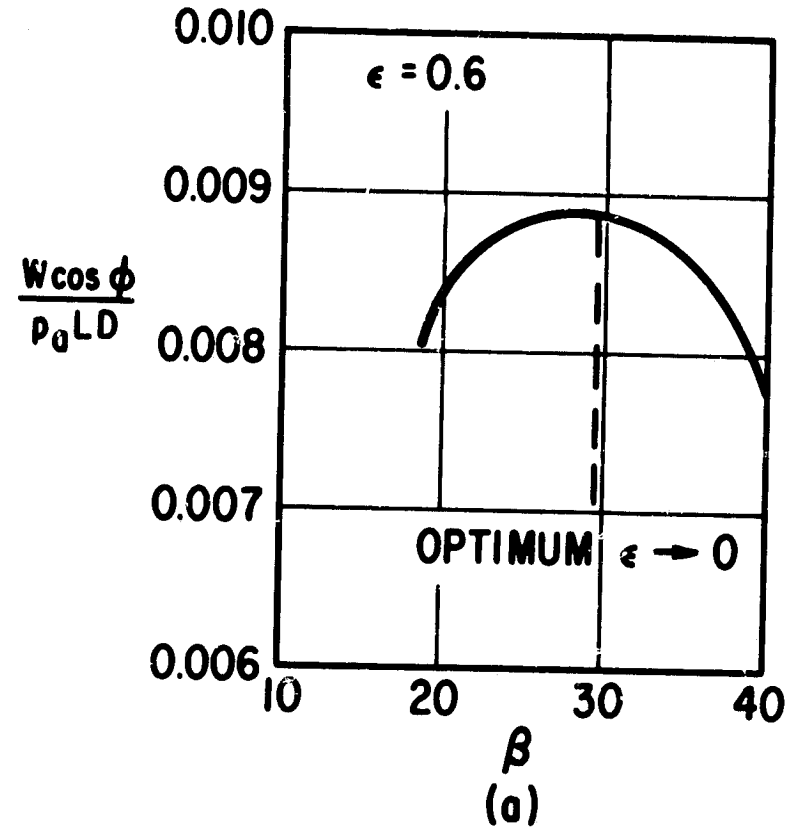

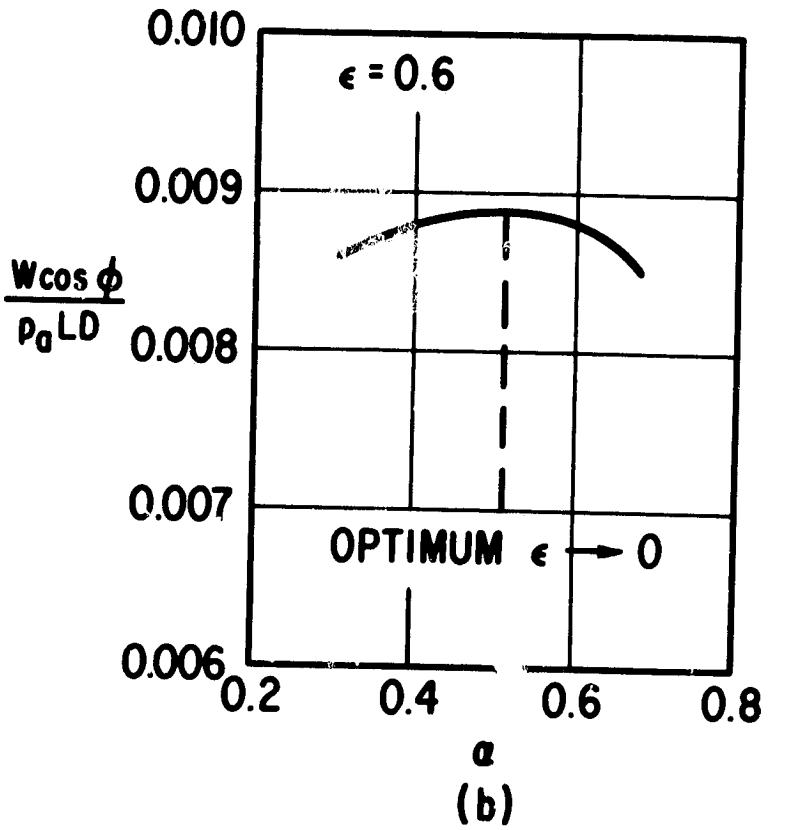

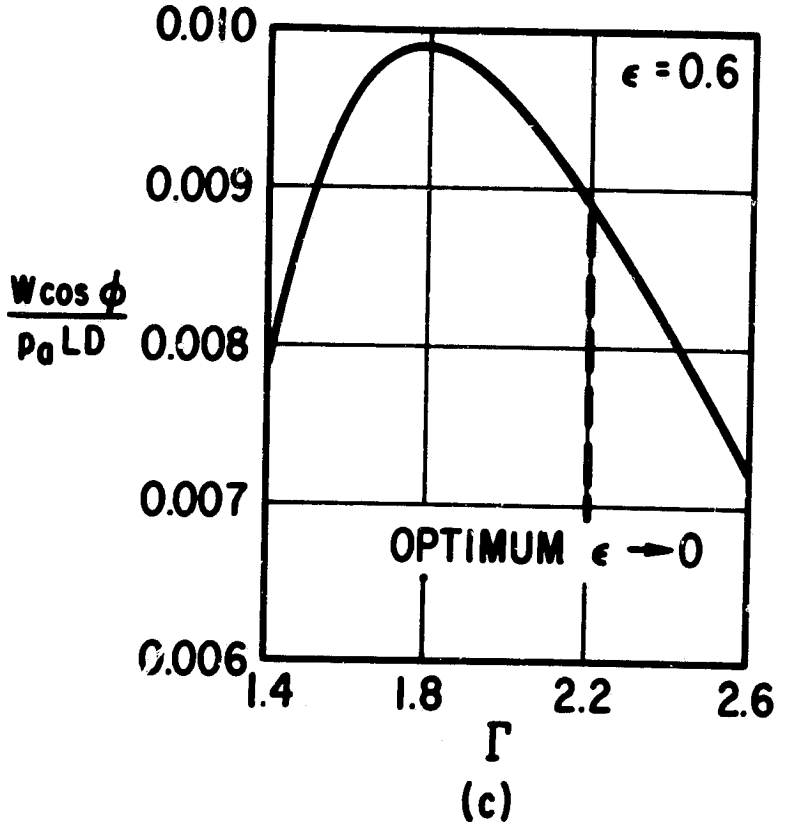

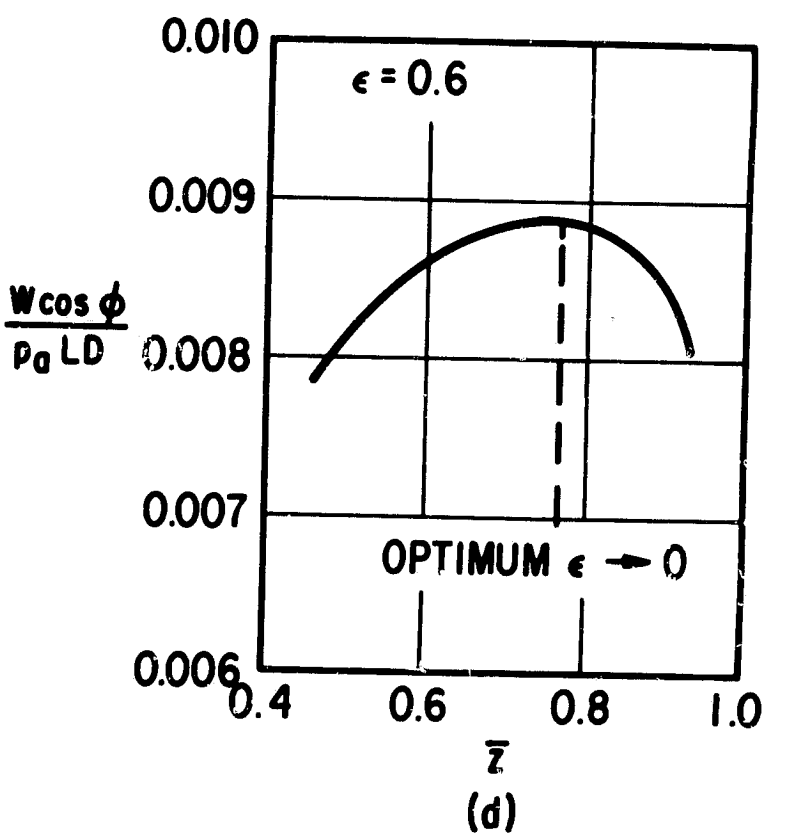

Fig. 8 Variation of Radial Load Capacity with Change in Groove Parameters at High Eccentricity

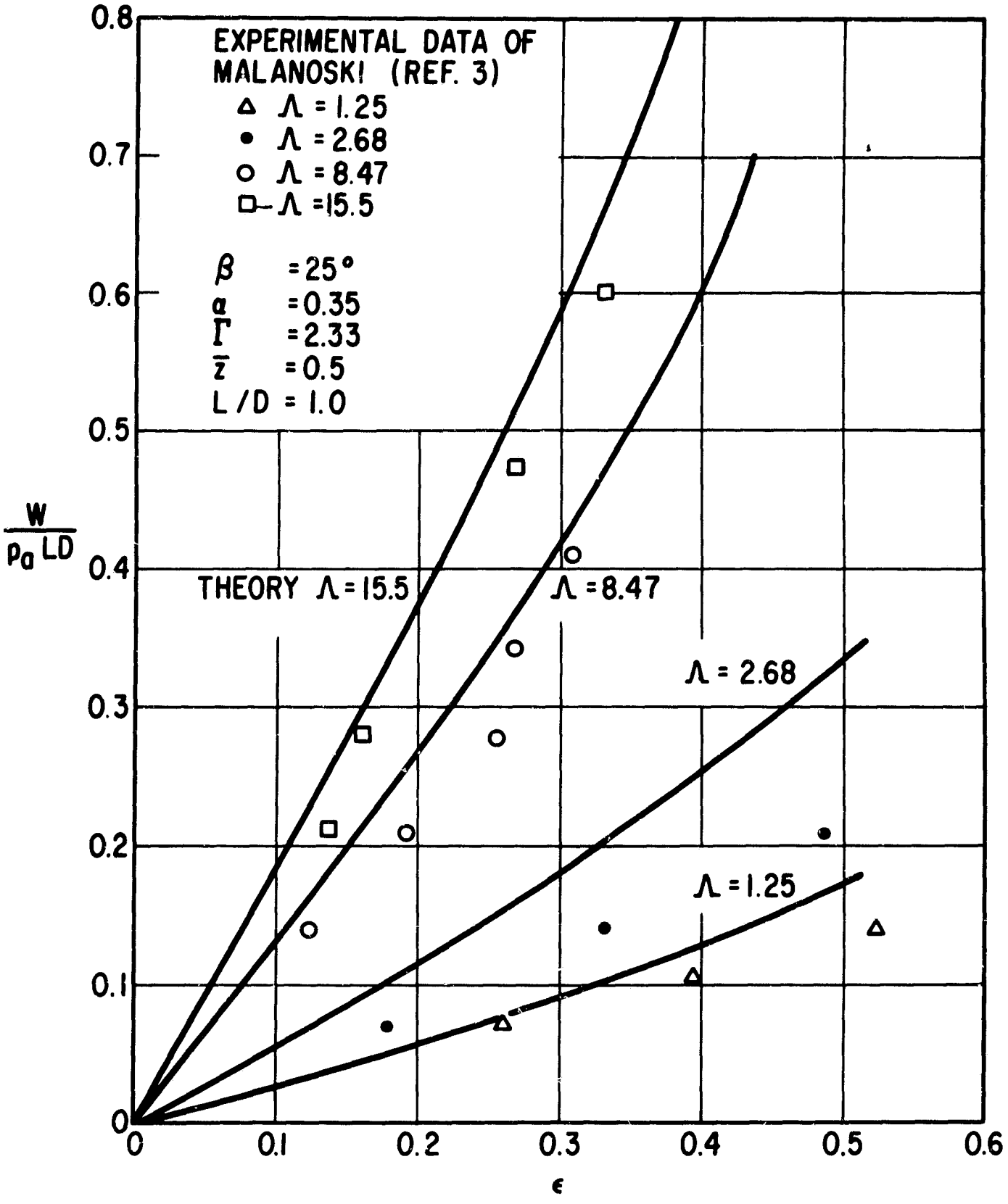

Fig. 9 Comparison of Theoretical Load with Experimental Data of Malanoski

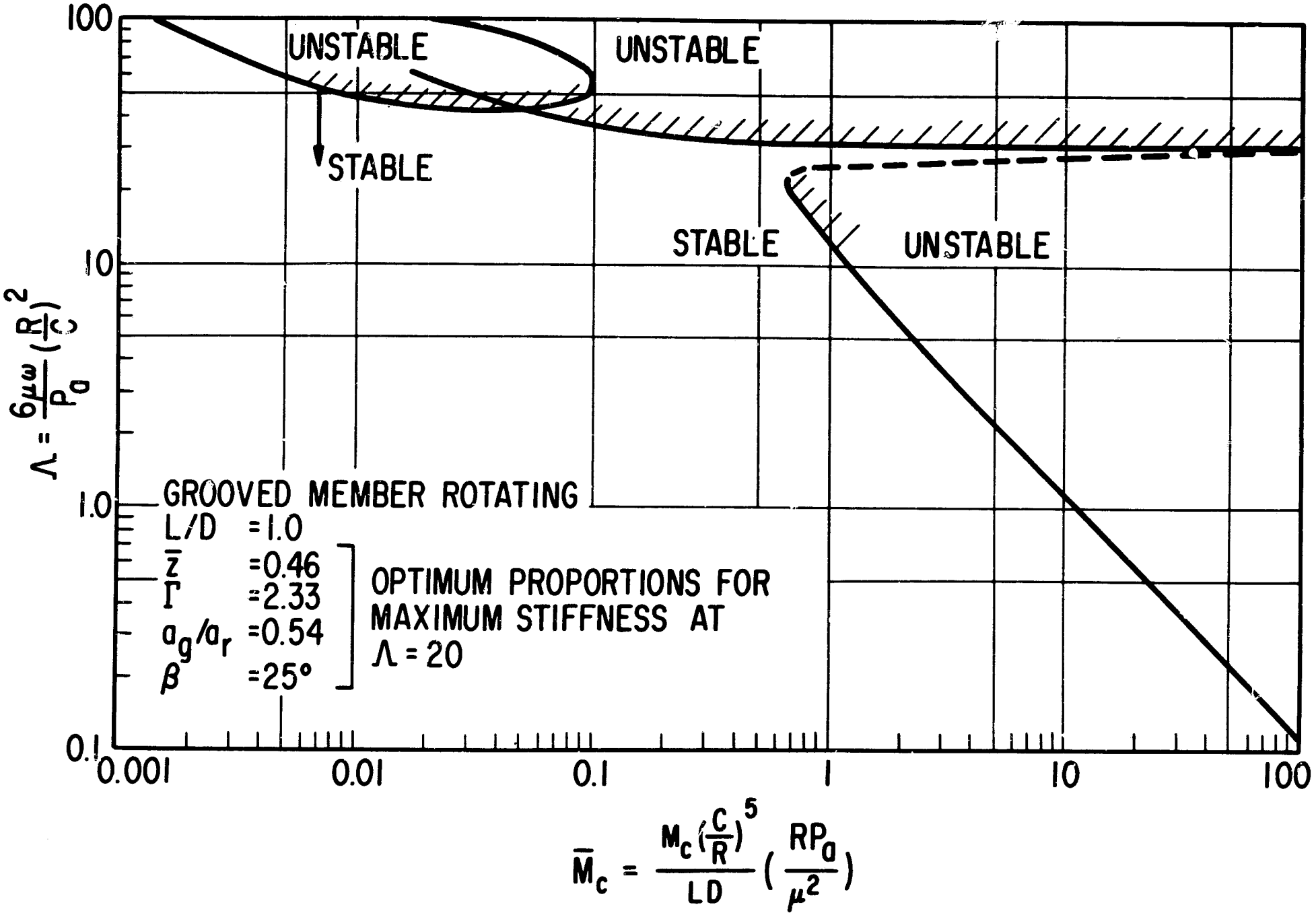

Fig. 10 Stability Map for Spiral-Grooved Bearing

MTI-3168

Security Classification

DOCUMENT CONTROL DATA - R&D

(Security classification of title, body of abstract and indexing annotation must be entered when the overall report is classified)

1. ORIGINATING ACTIVITY *(Corporate author)* Mechanical Technology Incorporated 968 Albany-Shaker Road Latham, New York 12110	2a. REPORT SECURITY CLASSIFICATION Unclassified 2b. GROUP None

3. REPORT TITLE

Performance Characteristics of Herringbone-Grooved Journal Bearings Operating at High Eccentricity Ratios and with Misalignment

4. DESCRIPTIVE NOTES *(Type of report and inclusive dates)*

Technical Report

5. AUTHOR(S) *(Last name, first name, initial)*

Castelli, V.
Vohr, J.H.

6. REPORT DATE	7a. TOTAL NO. OF PAGES	7b. NO. OF REFS
March, 1967	26	11

8a. CONTRACT OR GRANT NO. Nonr-3730(00)(FBM) b. PROJECT NO. RD-443 c. d.	9a. ORIGINATOR'S REPORT NUMBER(S) MTI-67TR15 9b. OTHER REPORT NO(S) *(Any other numbers that may be assigned this report)*

10. AVAILABILITY/LIMITATION NOTICES

Copies may be obtained by qualified requestors from DDC

11. SUPPLEMENTARY NOTES	12. SPONSORING MILITARY ACTIVITY
None	Office of Naval Research

13. ABSTRACT

The differential equation for the pressure distribution around a spiral-grooved journal bearing with compressible lubricant is solved by the numerical method of matrix influence coefficients for the case of arbitrary eccentricity and misalignment. Performance characteristics are presented for one particular bearing over the range $0 < \Lambda < 20$. Results are presented showing the restoring moment due to misalignment, the effect of L/D ratio at large eccentricity and the influence of eccentricity ratio on the optimum values of groove parameters for maximum radial stiffness. Comparision is made with experimental results.

DD FORM 1 JAN 64 1473

Security Classification

14. KEY WORDS	LINK A		LINK B		LINK C	
	ROLE	WT	ROLE	WT	ROLE	WT
Gas Bearings						
Spiral-Grooved Bearings						

INSTRUCTIONS

1. **ORIGINATING ACTIVITY:** Enter the name and address of the contractor, subcontractor, grantee, Department of Defense activity or other organization *(corporate author)* issuing the report.

2a. **REPORT SECURITY CLASSIFICATION:** Enter the overall security classification of the report. Indicate whether "Restricted Data" is included. Marking is to be in accordance with appropriate security regulatio .

2b. **GROUP:** Automatic downgrading i. specified in DoD Directive 5200.10 and Armed Forces Industrial Manual. Enter the group number. Also, when applicable, show that optional markings have been used for Group 3 and Group 4 as authorized.

3. **REPORT TITLE:** Enter the complete report title in all capital letters. Titles in all cases should be unclassified. If a meaningful title cannot be selected without classification, show title classification in all capitals in parenthesis immediately following the title.

4. **DESCRIPTIVE NOTES:** If appropriate, enter the type of report, e.g., interim, progress, summary, annual, or final. Give the inclusive dates when a specific reporting period is covered.

5. **AUTHOR(S):** Enter the name(s) of author(s) as shown on or in the report. Enter last name, first name, middle initial. If military, show rank and branch of service. The name of the principal author is an absolute minimum requirement.

6. **REPORT DATE:** Enter the date of the report as day, month, year; or month, year. If more than one date appears on the report, use date of publication.

7a. **TOTAL NUMBER OF PAGES:** The total page count should follow normal pagination procedures, i.e., enter the number of pages containing information.

7b. **NUMBER OF REFERENCES:** Enter the total number of references cited in the report.

8a. **CONTRACT OR GRANT NUMBER:** If appropriate, enter the applicable number of the contract or grant under which the report was written.

8b, 8c, & 8d. **PROJECT NUMBER:** Enter the appropriate military department identification, such as project number, subproject number, system numbers, task number, etc.

9a. **ORIGINATOR'S REPORT NUMBER(S):** Enter the official report number by which the document will be identified and controlled by the originating activity. This number must be unique to this report.

9b. **OTHER REPORT NUMBER(S):** If the report has been assigned any other report numbers *(either by the originator or by the sponsor)*, also enter this number(s).

10. **AVAILABILITY/LIMITATION NOTICES:** Enter any limitations on further dissemination of the report, other than those imposed by security classification, using standard statements such as:

(1) "Qualified requesters may obtain copies of this report from DDC."

(2) "Foreign announcement and dissemination of this report by DDC is not authorized."

(3) "U. S. Government agencies may obtain copies of this report directly from DDC. Other qualified DDC users shall request through

_____."

(4) "U. S. military agencies may o ain copies of this report directly from DDC. Other qualified users shall request through

_____."

(5) "All distribution of this report is controlled. Qualified DDC users shall request through

_____."

If the report has been furnished to the Office of Technical Services, Department of Commerce, for sale to the public, indicate this fact and enter the price, if known.

11. **SUPPLEMENTARY NOTES:** Use for additional explanatory notes.

12. **SPONSORING MILITARY ACTIVITY:** Enter the name of the departmental project office or laboratory sponsoring *(paying for)* the research and development. Include address.

13. **ABSTRACT:** Enter an abstract giving a brief and factual summary of the document indicative of the report, even though it may also appear elsewhere in the body of the technical report. If additional space is required, a continuation sheet shall be attached.

It is highly desirable that the abstract of classified reports be unclassified. Each paragraph of the abstract shall end with an indication of the military security classification of the information in the paragraph, represented as *(TS)*, *(S)*, *(C)*, or *(U)*.

There is no limitation on the length of the abstract. However, the suggested length is from 150 to 225 words.

14. **KEY WORDS:** Key words are technically meaningful terms or short phrases that characterize a report and may be used as index entries for cataloging the report. Key words must be selected so that no security classification is required. Identifiers, such as equipment model designation, trade name, military project code name, geographic location, may be used as key words but will be followed by an indication of technical context. The assignment of links, roles, and weights is optional.